Erciyes University Journal of Institute Of Science and Technology

Research Article
10.65520/erciyesfen.1990175

Imprint:
Volume: 42(3)
Year: 2026
Page: 396-418

Murat YEŞİL[a*]
Eda ŞENTÜRK[b]

[a]Prof. Dr., Ordu University, Faculty of Agriculture, Department of Landscape Architecture, Ordu, Türkiye.,
muraty25@hotmail.com
[b]MSc, Ordu University, Institute of Science and Technology, Department of Landscape Architecture, Ordu, Türkiye.
edasenturk653@gmail.com

* Corresponding Author

Received: 7/8/2026
Accepted: 9/28/2026

Citation:
Murat YEŞİL, Eda ŞENTÜRK (2026). Spatial Temporal Analysis of Impervious Surface Distribution at the Neighborhood Scale in the Urban Center: The Case of Ordu-Altınordu (Türkiye). *Erciyes University Journal of Institute Of Science and Technology*, 42(3), 396-418. https://doi.org/10.65520/erciyesfen.*1990175*

Screened by
iThenticate for Authors & Researchers

Except where otherwise noted, content in this article is licensed under a Creative Commons 4.0 International license. Icons by Font Awesome.

Spatial Temporal Analysis of Impervious Surface Distribution at the Neighborhood Scale in the Urban Center: The Case of Ordu-Altınordu (Türkiye)

Abstract

Background/Aim: The increasing replacement of natural surfaces with impervious surfaces due to rapid urbanization has significant spatial and environmental impacts on urban ecosystems. Therefore, monitoring the spatial distribution and temporal change of impervious surfaces is essential for understanding urban growth processes and supporting sustainable planning decisions. This study aimed to analyze the spatial distribution of impervious surfaces and their changes between 2015 and 2025 in 18 neighborhoods of Altınordu district (Ordu, Türkiye) using the Enhanced Normalized Difference Impervious Surface Index (ENDISI).

Methods: Sentinel-2 Level-2A satellite imagery acquired for 2015 and 2025 was used to calculate the ENDISI. Impervious surfaces were extracted using a threshold-based classification approach after preprocessing and water masking with the Modified Normalized Difference Water Index (MNDWI). Classification performance was evaluated using the Spectral Discrimination Index (SDI) and an error matrix-based accuracy assessment. In addition, neighborhood-level impervious surface proportions for 2015 and 2025 were statistically compared using the Wilcoxon signed-rank test.

Results: The results revealed an overall increase in impervious surface areas between 2015 and 2025. Neighborhood-scale analyses demonstrated that impervious surface change was spatially heterogeneous, with the magnitude of change varying considerably among the selected neighborhoods. The paired comparison confirmed a statistically significant difference in neighborhood-level impervious surface proportions between 2015 and 2025 ($p = 0.004$), with a large effect size ($r_{rb} = 0.84$). The classification achieved overall accuracies of 92.3% and 94.3%, with Kappa coefficients of 0.84 and 0.88 for 2015 and 2025, respectively.

Conclusion: The findings indicate that ENDISI provided satisfactory classification performance within the selected urban neighborhoods of Altınordu. The study offers a case-specific neighborhood-scale assessment of net impervious-surface change that can contribute to local urban monitoring and spatial planning evaluations.

Keywords: Remote sensing, Sentinel-2, Urban Growth, ENDISI, Impervious Surface

Kent Merkezinde Geçirimsiz Yüzeylerin Mahalle Ölçeğinde Mekânsal-Zamansal Dağılımının Analizi: Ordu-Altınordu (Türkiye) Örneği

Öz

Kentleşme süreçlerinin hızlanmasıyla birlikte doğal yüzeylerin yerini giderek artan oranda geçirimsiz yüzeylerin alması, kentsel ekosistemler üzerinde

önemli mekânsal ve çevresel etkiler oluşturmaktadır. Bu nedenle geçirimsiz yüzeylerin mekânsal dağılımının ve zamansal değişiminin izlenmesi, kentsel büyüme süreçlerinin anlaşılması ve sürdürülebilir planlama kararlarının desteklenmesi açısından önemlidir. Bu çalışmada, Ordu ili Altınordu ilçesindeki seçilmiş 18 kentsel mahallede geçirimsiz yüzeylerin mekânsal dağılımı ve 2015–2025 yılları arasındaki değişimi, Geliştirilmiş Normalleştirilmiş Fark Geçirimsiz Yüzey İndeksi (ENDISI) kullanılarak analiz edilmiştir. Çalışmada 2015 ve 2025 yıllarına ait Sentinel-2 Level-2A uydu görüntüleri kullanılmış; ön işleme ve Modifiye Edilmiş Normalleştirilmiş Fark Su İndeksi (MNDWI) ile su yüzeylerinin maskelenmesinin ardından geçirimsiz yüzeyler eşik değerine dayalı sınıflandırma yaklaşımıyla belirlenmiştir. Sınıflandırma performansı Spektral Ayrım İndeksi (SDI) ve hata matrisi temelli doğruluk değerlendirmesiyle incelenmiştir. Ayrıca 2015 ve 2025 yıllarına ait mahalle ölçeğindeki geçirimsiz yüzey oranları Wilcoxon işaretli sıralar testi kullanılarak istatistiksel olarak karşılaştırılmıştır. Bulgular, 2015–2025 döneminde geçirimsiz yüzey alanlarında genel bir artış olduğunu ve değişimin seçilmiş mahalleler arasında mekânsal olarak heterojen bir yapı gösterdiğini ortaya koymuştur. Eşleştirilmiş karşılaştırma sonucunda, 2015 ve 2025 yıllarındaki mahalle ölçeğindeki geçirimsiz yüzey oranları arasında istatistiksel olarak anlamlı bir fark belirlenmiş ($p = 0,004$) ve etki büyüklüğünün yüksek olduğu saptanmıştır ($r_{rb} = 0,84$). Sınıflandırmada 2015 ve 2025 yılları için sırasıyla %92,3 ve %94,3 genel doğruluk ile 0,84 ve 0,88 Kappa katsayıları elde edilmiştir. Sonuçlar, ENDISI'nin Altınordu'da seçilmiş kentsel mahalleler kapsamında geçirimsiz yüzeylerin belirlenmesinde tatmin edici bir sınıflandırma performansı sağladığını göstermektedir. Çalışma, Altınordu'da mahalle ölçeğindeki net geçirimsiz yüzey değişiminin izlenmesine ve yerel mekânsal planlama değerlendirmelerine katkı sağlayabilecek alana özgü ampirik bulgular sunmaktadır.

Anahtar kelimeler: Uzaktan Algılama, Sentinel-2, Kentsel Büyüme, ENDISI, Geçirimsiz Yüzey

1. INTRODUCTION

Accelerating population growth and associated spatial expansion since the 20th century has led to an increase in the number of roads, roofs, pavements and other artificial surfaces, leading to an increase in impervious surfaces [1,40]. Impervious surfaces are generally defined as artificial surfaces that prevent rainwater from seeping into the ground and are largely formed as a result of human activities [2]. These surfaces mainly include building roofs, asphalt and concrete covered roads, parking areas, sidewalks and transportation infrastructure systems [3]. This transformation does not only refer to the physical change in land cover. It also creates versatile ecological and hydrological effects on the urban environment. The increase in impervious surfaces that limit the infiltration of rainwater into the ground causes an increase in the risk of urban floods and also contributes to the strengthening of the urban heat island effect [4-7]. In addition, the increase in impervious surfaces leads to the fragmentation of natural habitats, weakening ecosystem continuity and limiting the mobility of biological species [8,9]. Therefore, determining the spatial distribution of impervious surfaces accurately and reliably constitutes an important research area in terms of understanding urban environmental dynamics and developing sustainable land use policies.

Multispectral satellite images allow the distinction of impervious and permeable surfaces by taking advantage of the spectral reflectance properties of different land cover components. In this context, subpixel-based approaches such as spectral mixture analysis [10-12], statistical methods such as decision tree and regression models [13] and various classification algorithms have been widely applied to determine impervious surfaces. However, the accuracy of these methods. The spatial resolution of the data set used may vary depending on factors such as land cover diversity and spectral mixing level in the study area. For this reason, spectral index-based approaches, which have the capacity to produce fast and comparable results especially in large areas, are widely preferred in determining impervious surfaces [11]. These approaches aim to distinguish built-up surfaces from other land cover classes by taking advantage of the reflectance differences between different spectral bands and show effective results in many studies. For example, Sentinel-2 satellites can be widely used in the analysis of urban impervious surfaces thanks to 10 m and 20 m spatial resolution bands.

Sentinel-2 satellites provide multispectral images with different spatial resolutions thanks to the MSI (MultiSpectral Instrument) sensor with 13 spectral bands covering the visible, near infrared and shortwave infrared regions [14,36,41]. This data set provides significant advantages in monitoring land cover components thanks to the band structure it provides at different spatial resolutions. In

CC: BY-NC-ND

particular, band combinations that allow spectral discrimination of vegetation, bare soil, water surfaces and built-up areas make Sentinel-2 images an effective data source in impervious surface analysis [15-18]. For this reason, in recent years, Sentinel-2 images have been widely used in studies on determining impervious surfaces [19-21].

Spectral indices developed for the determination of impervious surfaces may show varying performances in different work areas. It is stated that some indices, especially the Biophysical Composition Index (BCI) and Combinational Build-up Index (CBI), are significantly affected by water surfaces, and commonly used indices such as the Index-based Built-up Index (IBI), Combinational Biophysical Composition Index (CBCI), and Normalized Difference Built-up Index (NDBI) may show differences in classification accuracy depending on the land cover characteristics of the study area [22]. On the other hand, it is stated that the Enhanced Normalized Difference Impervious Surface Index (ENDISI) produces more stable results in areas with different land cover conditions and provides higher discrimination performance in determining impervious surfaces. Comparative studies have shown that the ENDISI algorithm has higher discrimination power than other indices and can reach overall accuracy values of over 91% [22,24]. Due to these features, the ENDISI index is considered to offer an effective approach in determining impervious surfaces quickly and reliably and monitoring temporal changes using Sentinel-2 images. Previous ENDISI and Sentinel-2 based studies and the urban contexts in which they were conducted are summarized in Table 1.

Table 1. Comparison of ENDISI and Sentinel-2 based impervious surface studies in terms of study area and urban context

Study	**Research area/region**	**Urban context and scale**	**Data, index and reported performance**
Chen et al. (2020) [22]	Multiple cities, China	Large and densely built cities	Sentinel-2; Index comparison including ENDISI; OA > 91%
Kebede et al. (2022) [15]	Addis Ababa, Ethiopia	Large metropolitan area	Sentinel-2A; Comparison of built-up indices
Dvornikov et al. (2023) [17]	Multi-latitude (global examples)	Different climates and urban textures	Sentinel-2; optimal index and threshold value analysis
Yücer (2025) [24]	Ankara, Türkiye	Large metropolitan area	Identifying impervious surfaces with remote sensing indices
Kuc & Chormański (2019) [29]	Warsaw, Poland	Large city	Sentinel-2; imperviousness mapping and monitoring
This study (2026)	Altınordu (Ordu), Türkiye	Medium-sized, coastal district with relatively low population density	Sentinel-2; ENDISI; neighborhood scale; OA 92–94%

This study aims to determine the spatial distribution and temporal change of impervious surfaces in the neighborhoods in Altınordu district center of Ordu province, which is a coastal settlement and exhibits heterogeneous land cover characteristics. In this context, ENDISI was calculated using Sentinel-2 satellite images of 2015 and 2025 and comparative analyses were carried out at the neighborhood scale.

In the literature, it is seen that studies carried out with ENDISI and similar spectral indices are largely carried out in large populated cities (Table 1). On the other hand, previous studies have demonstrated the applicability of ENDISI and related impervious-surface indices across different

CC: BY-NC-ND

urban and environmental contexts, including large and densely built cities, plateau-basin environments, coastal cities, and other heterogeneous urban areas [15-17,19,29,30,32,33]. However, comparatively fewer studies have emphasized neighborhood-scale differences in net impervious-surface change within medium-sized coastal urban settings. Accordingly, the present study does not seek to establish a new spectral-index methodology, but rather to extend the empirical application of ENDISI to a neighborhood-scale assessment in Altınordu. Altınordu constitutes a suitable sample area representing this gap, as it combines the concentrated construction along the coastal zone with the sloping and heterogeneous land cover in the interior. For this reason, in the study, determining the spatial distribution and net temporal change between 2015 and 2025 of impervious surfaces on a neighborhood basis was considered as a research question. Answering this question is important for understanding neighborhood-level spatial differences in impervious surface change and supporting local spatial planning assessments. The aim of this study is not to compare different impervious surface indices, but to reveal the spatial-temporal change at the neighborhood scale using the ENDISI index, whose accuracy has been shown in the literature. The main contribution of this study lies in its case-specific, neighborhood-scale empirical assessment of impervious surface change in Altınordu using the established ENDISI approach. Rather than proposing a new methodological framework, the study applies existing remote-sensing procedures to examine how net impervious surface change between 2015 and 2025 varies among selected urban neighborhoods within a medium-sized coastal settlement. This neighborhood-level focus provides spatially detailed evidence that may support local-scale urban monitoring and planning assessments.

The main research question of the study is how the spatial distribution of impervious surfaces in Altınordu district center and the change patterns in the period 2015–2025 developed on a neighborhood basis. In this regard, the study aims to evaluate neighborhood-level differences in impervious surface change and discuss their implications for local urban monitoring and spatial planning.

2. RESEARCH AREA

Within the scope of this study, the neighborhood-scale analysis was restricted to 18 neighborhoods comprising the main urban settlement belt of Altınordu district center (Figure 1). The term “main urban settlement belt” refers to an operational spatial extent defined for the purposes of this study rather than to an independently designated administrative or statutory planning boundary. The 18 neighborhoods were selected based on the spatial continuity and concentration of built-up areas within the coastal and central urban zone, while the numerous predominantly rural neighborhoods within the wider administrative territory of Altınordu were excluded from the urban-focused analysis. This delineation was established independently of the magnitude of impervious-surface change observed between 2015 and 2025. Accordingly, the temporal comparisons presented in this study refer specifically to these 18 selected urban neighborhoods and should not be generalized to the entire Altınordu district.

CC: BY-NC-ND

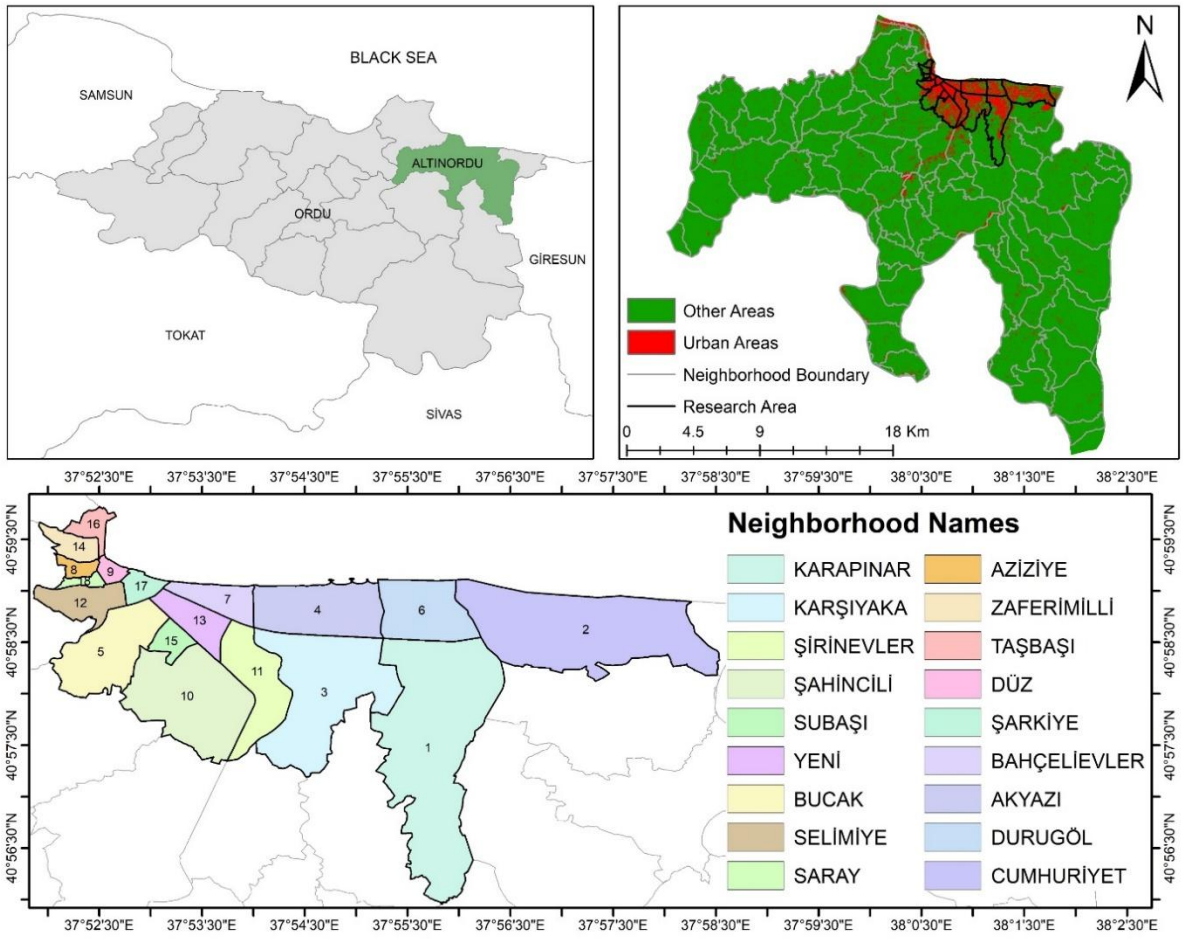

Figure 1. Location of Altınordu district of Ordu province, district center study area border and spatial distribution of 18 neighborhoods evaluated within the scope of the analysis.

Altınordu district has experienced substantial spatial transformation in recent years within the broader context of population growth, transportation infrastructure development, and urban activities concentrated along the coast. This process may be associated with the observed patterns of construction density and impervious surface distribution, particularly in the coastal and central parts of the district. The combination of residential areas developed along the coastal zone and sloping topographic conditions in the inner parts makes the study area a suitable sample area for examining the spatial distribution of impervious surfaces.

3. MATERIALS AND METHODS

The spatial distribution and temporal changes of the impervious surfaces of 18 neighborhoods in Altınordu district center were analyzed with the Enhanced Normalized Difference Impervious Surface Index (ENDISI) applied to Sentinel-2 satellite images. In the first stage, ENDISI distributions for the years 2015 and 2025 were examined, and then impervious surface classes were created in line with the determined threshold value. The classification results obtained were evaluated on a neighborhood scale, impervious surface areas were calculated for each neighborhood, and the change between the two periods was analyzed comparatively. In addition, the discrimination performance of the index between classes was evaluated using the Spectral Discrimination Index (SDI), and the classification accuracy was revealed by error matrix-based accuracy analysis. Natural color composite (Band 4–3–2) obtained from Sentinel-2 images was used to support the visual evaluation of impervious surface change in selected sample neighborhoods. Finally, the statistical significance of the temporal change in neighborhood-level impervious surface proportions between 2015 and 2025 was evaluated using paired statistical analysis (Figure 2).

CC: BY-NC-ND

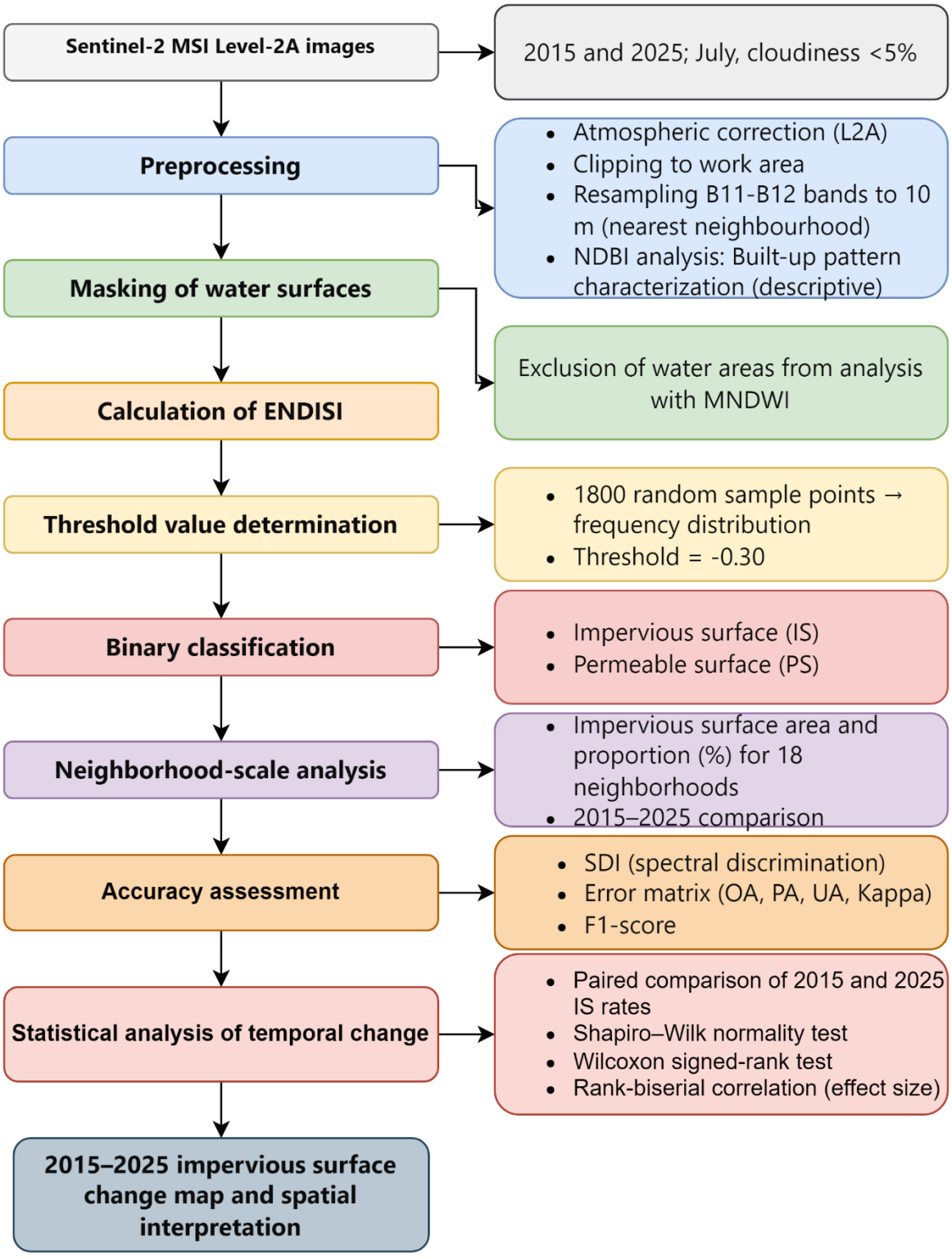

Figure 2. Methodological workflow followed in the study

3.1. Sentinel-2A Satellite Data

In order to spatially reveal the density of construction in the study area, Normalized Difference Built-up Index (NDBI) derived from Sentinel-2 satellite images of 2025 was used. NDBI, which takes advantage of the spectral reflectance differences of built-up areas in the shortwave infrared (SWIR)

and near infrared (NIR) bands, is calculated with the following equation:

$$\text{NDBI} = \frac{\text{SWIR1}-\text{NIR}}{\text{SWIR1}+\text{NIR}} \quad (1)$$

In Sentinel-2 images, the SWIR1 band is represented by B11 and the NIR band is represented by B8. The 2025 NDBI map was used as supplementary spatial information to characterize the concentration and spatial distribution of built-up areas within the defined urban settlement belt. The neighborhood-scale analysis was restricted to 18 neighborhoods comprising the previously defined main urban settlement belt of Altınordu. The selection was based on the spatial continuity and concentration of built-up areas within the coastal and central urban zone, independently of the magnitude of impervious surface change observed between 2015 and 2025. Within this predefined urban extent, the NDBI map was used only as supplementary spatial information to characterize the distribution and concentration of built-up surfaces and was not used as a criterion for selecting neighborhoods according to their subsequent temporal change. Accordingly, the analysis represents the selected urban settlement belt rather than the entire administrative district of Altınordu.

Level-2A surface reflectance images obtained by the MSI sensor of the Sentinel-2 satellite were used to determine the spatial distribution and temporal change of impervious surfaces. Sentinel-2 images consist of a total of 13 spectral bands and provide data at 10 m, 20 m and 60 m spatial resolutions depending on the band characteristics.

Sentinel-2 images acquired in July 2015 and July 2025, each with a cloud cover of less than 5%, were used to determine impervious surface change in the study area.

Sentinel-2 bands used in the study, their spatial resolutions and their intended use in the analysis process are given in Table 2. Relevant spectral bands were used to calculate the ENDISI, MNDWI and NDBI indices. In addition, RGB bands were used for the natural color composite to make visual evaluation in selected sample areas.

Table 2. Sentinel-2 spectral bands, spatial resolutions, and intended uses in the analysis

Band	Pixel size(m)	Intended use
B2- Blue	10	ENDISI- RGB
B3-Green	10	MNDWI- RGB
B4-Red	10	RGB
B8-NIR	10	NDBI
B11-$SWIR_1$	20	MNDWI- ENDISI- NDBI
B12-$SWIR_2$	20	ENDISI

3.2. Pre-Processing Process

Sentinel-2 images were subjected to pre-processing steps before analysis and were made suitable for the study area and index calculations. In this context, atmospherically corrected Level-2A surface reflectance data was used and the images were cut according to the boundaries of the study area. In Sentinel-2 images, B2, B3 and B8 bands have a spatial resolution of 10 m, while B11 and B12 bands have a spatial resolution of 20 m. For this reason, in order to ensure spatial resolution compatibility between the bands in the calculation of the ENDISI index, B11 and B12 bands were converted to 10 m spatial resolution by using the nearest neighbor resampling method in the ArcMap environment. Thus, it was ensured that the bands used in index calculations were evaluated at the same spatial resolution.

3.3. Masking of Water Surfaces (MNDWI)

Since water surfaces can show spectral similarity to impervious surfaces, MNDWI-based masking was applied as a preprocessing step to minimize the potential for misclassification between water and impervious surfaces.

$$\text{MNDWI} = \frac{\text{Green}-\text{SWIR1}}{\text{Green}+\text{SWIR1}} \quad (2)$$

CC: BY-NC-ND

The obtained MNDWI raster data was classified using the determined threshold value and water surfaces were excluded from the analysis.

3.4. Calculation of ENDISI

The Enhanced Normalized Difference Impervious Surface Index (ENDISI) was used to determine impervious surfaces:

$$\text{ENDISI} = \frac{\text{Blue} - \alpha \times (\frac{\text{SWIR1}}{SWIR2}) + (MNDWI \times MNDWI)}{\text{Blue} + \alpha \times (\frac{\text{SWIR1}}{SWIR2}) + (MNDWI \times MNDWI)} \quad (3)$$

Here, the coefficient α was calculated using the following equation:

$$a = \frac{\text{Mean(Blue)}}{(\frac{\text{SWIR1}}{SWIR2}) Mean + (MNDWI \times MNDWI) Mean} \quad (4)$$

3.5. Determination of Threshold Value

Selecting a threshold value to distinguish between impervious and permeable surfaces using ENDISI values constitutes an important step in the classification process. In this study, a sampling-based approach was employed to determine the threshold value. For a total of 1800 sample points randomly distributed across the study area, the corresponding ENDISI values were extracted from the 2025 ENDISI image using the "Extract Values to Points" tool. These sample points formed the threshold-determination dataset and were generated independently of the reference points used later for accuracy assessment. The frequency distribution of the obtained ENDISI values was examined using a histogram. Based on the observed transition between lower ENDISI values associated with permeable surfaces and higher values associated with impervious surfaces, a threshold value of −0.30 was selected through visual inspection of the empirical distribution. No automated threshold-optimization algorithm or predefined quantitative criterion was applied. This study-specific threshold is consistent with recent evidence indicating that ENDISI thresholds may require adjustment according to local spectral and land-cover characteristics. Li et al. (2026) reported that statistical analyses of representative samples showed that ENDISI values for built-up areas were predominantly distributed between −0.30 and 0.20, leading to the adoption of ENDISI > −0.30 as the criterion for impervious-surface classification [46]. Accordingly, the −0.30 value used in the present study should be interpreted as an empirically selected, study-specific decision threshold rather than as a universal ENDISI threshold. The classification performance of this threshold was subsequently evaluated using an independent reference dataset through the accuracy-assessment procedure described in Section 3.6.2.

A common threshold value of −0.30 was applied to the ENDISI images for both 2015 and 2025 to maintain a consistent classification criterion across the two observation dates. Rather than using different year-specific thresholds, the same decision boundary was retained to avoid introducing artificial temporal differences resulting from changes in the classification threshold. The temporal applicability of this common threshold was subsequently evaluated independently for each year through accuracy assessment. The resulting overall accuracy values of 92.3% for 2015 and 94.3% for 2025, together with Kappa coefficients of 0.84 and 0.88, respectively, indicate satisfactory classification performance for both periods.

3.6. Performance Evaluation

It may not be sufficient to base the performance of impervious surface indices solely on visual evaluation. Therefore, it is important to evaluate the index results in terms of quantitative accuracy and discriminatory power. It is stated in the literature that the performance of impervious surface indices can be evaluated with Spectral Discrimination Index (SDI) and error matrix-based accuracy analysis approaches [25]. Within the scope of this study, SDI and error matrix based accuracy analysis was applied to evaluate the performance of impervious surface index results.

CC: BY-NC-ND

3.6.1. Spectral Discrimination Index (SDI)

Spectral Discrimination Index (SDI) was calculated to evaluate the performance of the ENDISI index in distinguishing impervious and permeable surfaces:

$$SDI = \frac{\mu 1 - \mu 2}{\sigma 1 + \sigma 2} \quad (5)$$

μ1 and μ2 are the average index values for the classes of impervious surface areas and other areas, respectively, and σ1 and σ2 are the standard deviations for the two classes [26]. According to the spectral discrimination scale, if SDI < 1, it is classified as "poor" since the classes overlap spectrally, if 1 ≤ SDI < 3, it is classified as "good" and if SDI ≥ 3, it is classified as "very good" [27].

3.6.2. Error Matrix

Error matrix-based accuracy analysis was performed to quantitatively evaluate the accuracy of impervious surface classification obtained using the ENDISI index. Accuracy assessment was based on comparison of impervious surface and permeable/other surface classes obtained as a result of classification with reference data.

For the accuracy assessment, a separate set of 1800 reference points was randomly distributed within the study area. This reference dataset was generated in a sampling procedure independent of the 1800 points used for threshold determination, so that the two datasets share no common points. High-resolution historical imagery available through Google Earth was used as reference data for the visual interpretation and classification of these points. Imagery from July 2015 and July 2025 was examined for the 2015 and 2025 accuracy assessments, respectively, to provide temporal correspondence with the Sentinel-2 observation periods used in the classification analysis. Because the underlying imagery source and nominal spatial resolution of the Google Earth historical imagery could not be consistently identified from the available records, these characteristics are not reported as fixed values.

The same 1800 reference-point locations were used for both observation dates, and each point was visually interpreted separately for 2015 and 2025 using the corresponding Google Earth imagery; the reference class assigned to a given location was therefore determined independently for each year according to the land-cover condition observed at that date. Each point was assigned to one of two classes: impervious surfaces (IS), covering building roofs, roads, parking areas, hard grounds and other artificial surfaces, and permeable/other surfaces (PS), covering natural and semi-natural surfaces such as vegetation, bare soil, open green areas and other non-impervious land-cover types.

Thus, a direct dependency between threshold value selection and accuracy evaluation is prevented. By comparing the reference classes and ENDISI-based classification results, a separate error matrix was created for both periods. Producer's accuracy, user's accuracy, overall accuracy, the Kappa coefficient and the F1-score were calculated from the error matrix.

Producer's accuracy shows how accurately the samples of a class determined in the reference data are represented as a result of classification. User's accuracy refers to the reliability of pixels assigned to a certain class as a result of classification actually belonging to that class. Overall accuracy shows the ratio of correctly classified samples to the total reference samples. Kappa coefficient reveals to what extent classification success differs from random agreement.

In addition, the F1-score was calculated in order to evaluate class-based accuracy performance more balanced. The F1-score is the harmonic mean of producer's accuracy and user's accuracy and contributes to the interpretation of class-based performance, particularly in two-class classifications.

The accuracy analysis carried out in this direction enabled the evaluation of ENDISI-based impervious surface classification based not only on visual interpretations but also on quantitative performance indicators.

$$\kappa = \frac{N \sum_{i=1}^{r} X_{ii} - \sum_{i=1}^{r} (X_i + X_{+i})}{N^2 - \sum_{i=1}^{r} (X_i + X_{+i})} \quad (6)$$

CC: BY-NC-ND

N is the total number of reference pixels, r is the number of classes (number of rows and columns), Xii i. line and i. value in column (diagonal value), Xi+ i. row sum and X+i i. is the column sum [28].

With the accuracy analysis carried out in this context, the reliability of the impervious surface classification obtained using ENDISI was evaluated quantitatively.

3.7. Statistical Analysis of Temporal Change

To evaluate whether the temporal change in impervious surface proportions between 2015 and 2025 was statistically significant, the impervious surface percentages obtained for the 18 neighborhoods were analyzed as paired observations. For each neighborhood, the temporal difference was calculated by subtracting the 2015 impervious surface percentage from the corresponding 2025 value (2025 − 2015). The normality of the paired differences was assessed using the Shapiro–Wilk test. Since the normality assumption was not satisfied, the non-parametric Wilcoxon signed-rank test was used to compare the impervious surface proportions between the two periods. Statistical significance was evaluated at an alpha level of 0.05 ($\alpha = 0.05$). Of the 18 paired neighborhood observations, three exhibited zero differences between 2015 and 2025 and were therefore excluded from the rank calculation, resulting in 15 non-zero pairs included in the Wilcoxon signed-rank test. In addition to statistical significance, rank-biserial correlation was calculated to quantify the effect size of the temporal change. All statistical analyses were performed using Jamovi 2.3.

3.8. Ethical Approval: Ethical approval is not required for this study

4. RESULTS

ENDISI-based spatial distribution maps show that impervious surfaces in the study area exhibit a distinct spatial pattern (Figure 3). When the ENDISI distribution for 2015 is examined, it is seen that high index values are concentrated mainly in the city center and coastal areas. It is noteworthy that red and orange tones are dominant, especially in neighborhoods with dense construction, while low index values (blue tones) are located in areas where urban development is limited.

Visual comparison of the ENDISI distribution maps indicates that high index values became more spatially extensive in 2025 compared with 2015, particularly within the central and coastal parts of the selected study area. These patterns are based on visual interpretation of the ENDISI maps and should not be interpreted as the result of a formal directional or corridor analysis. On the other hand, it is understood that the permeable surfaces represented by low index values are more concentrated in the peripheral areas.

CC: BY-NC-ND

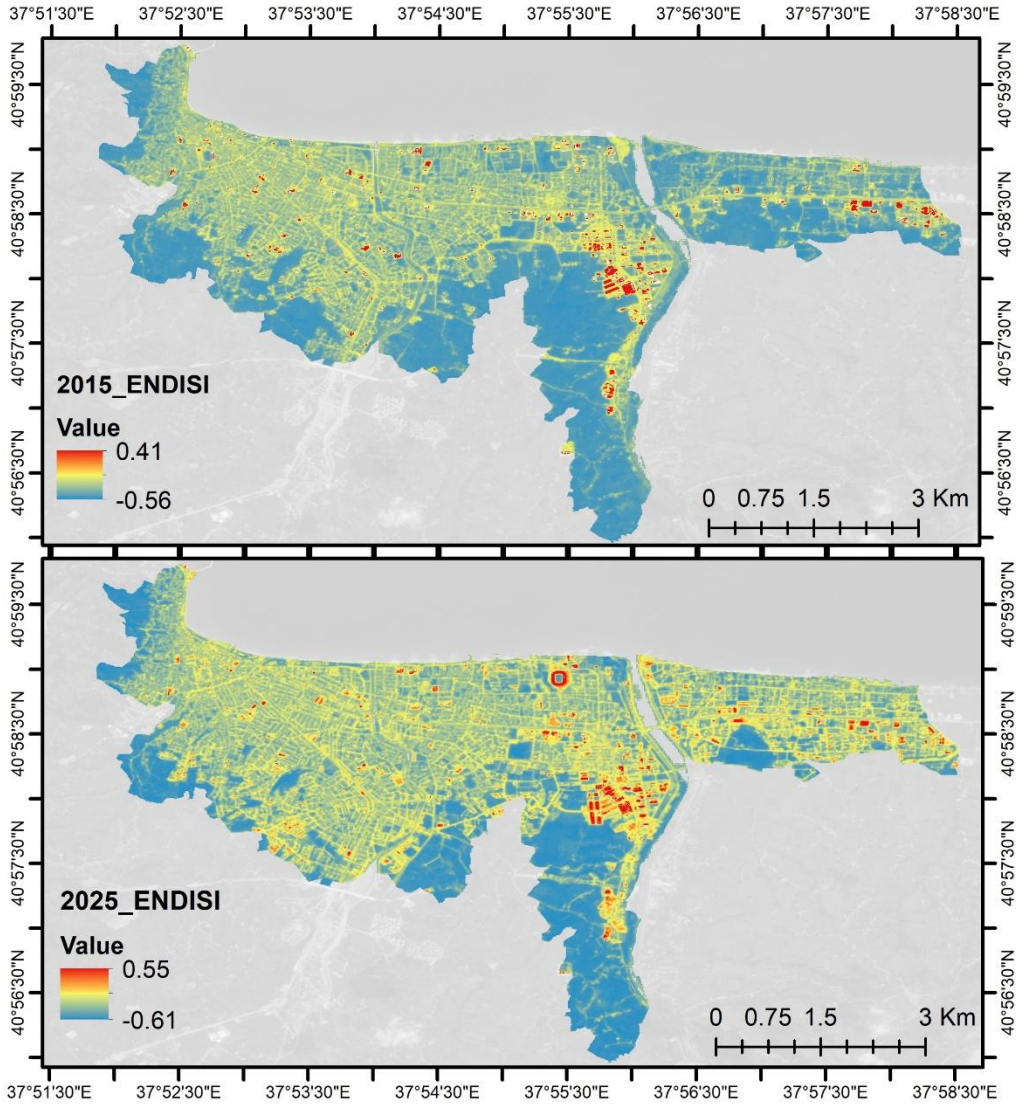

Figure 3. 2015–2025 ENDISI Index Results

The frequency distribution of the ENDISI values extracted from the 2025 sample points is presented in Figure 4. Visual inspection of the empirical frequency distribution indicated a transition around −0.30 between lower ENDISI values associated with permeable surfaces and higher values associated with impervious surfaces. Accordingly, −0.30 was adopted as the classification threshold for 2025 and applied unchanged to the 2015 ENDISI image to maintain a consistent decision criterion between the two observation dates. As described in Section 3.5, this threshold was selected empirically from the 2025 frequency distribution rather than through an automated threshold-optimization procedure. Because the two classes displayed in Figure 4 are delineated using the applied threshold, the figure illustrates the resulting class distributions rather than providing independent validation of the threshold value. Independent empirical support for the classification performance of this common threshold is therefore provided by the year-specific, reference-based accuracy assessments reported below (Tables 3 and 4).

CC: BY-NC-ND

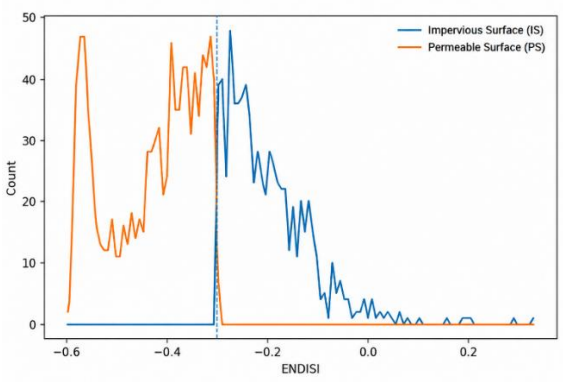

Figure 4. Frequency distribution of ENDISI values at the 2025 sample points and the −0.30 decision boundary

ENDISI raster data was classified in line with the determined threshold value and impervious and permeable surfaces were separated. The binary classification obtained as a result of this process allowed the spatial distribution of impervious surfaces in the study area to be revealed more clearly. The classification results obtained formed the basic data set for the analyses carried out at the neighborhood scale (Figure 5).

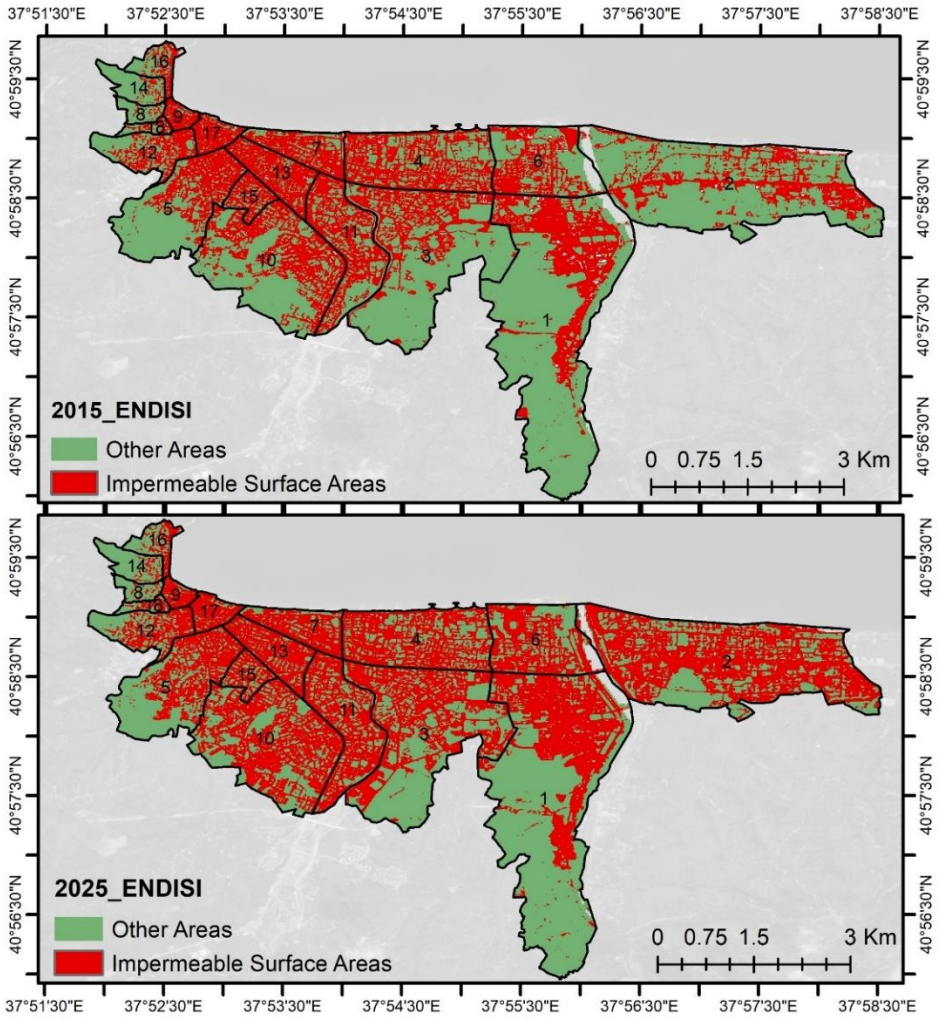

Figure 5. Impervious surface areas according to ENDISI Index results

SDI and error matrix approaches from validation samples, which show the spectral separation between impervious surface areas and other areas, were used for performance evaluation of impervious surface indices. In the accuracy evaluation, producer's accuracy, user's accuracy, overall accuracy, the Kappa coefficient and the F1-score were calculated from the error matrix constructed with 756 reference points for impervious surface areas and 1044 reference points for other areas (Table 3).

Table 3. SDI values and Error matrix

	Feature	SDI	PA	UA
2015	Impervious surface areas	1.36	0.94	0.88
	Other areas		0.91	0.95
			OA = 0.923	κ = 0.84
2025	Impervious surface areas	1.48	0.96	0.91
	Other areas		0.93	0.97
			OA = 0.943	κ = 0.88

Error matrix results (Table 4) reveal high classification accuracy for both periods. The accuracy assessment yielded overall accuracies of 92.3% and 94.3% and Kappa coefficients of 0.84 and 0.88 for 2015 and 2025, respectively. The corresponding F1-scores were 0.91 for the impervious surface class and 0.93 for the permeable/other surface class in 2015, and 0.93 and 0.95, respectively, in 2025. According to the SDI results, the spectral discrimination power was 1.36 for 2015 and 1.48 for 2025. Both values fall within the same SDI performance category ($1 \leq SDI < 3$), indicating satisfactory spectral discrimination between the classes in both periods. Although the SDI value was numerically higher in 2025, the present analysis does not identify the factors responsible for this difference.

Table 4. Error matrix for ENDISI-based classification (2015 and 2025)

	Reference: Impervious (IS)	**Reference: Other (PS)**	**Total (class)**	**UA**
2015				
Class: IS	711	94	805	0.88
Class: PS	45	950	995	0.95
Total	756	1044	1800	
PA	0.94	0.91	OA=0.923	
	Reference: Impervious (IS)	**Reference: Other (PS)**	**Total (class)**	**UA**
2025				
Class: IS	726	73	799	0.91
Class: PS	30	971	1001	0.97
Total	756	1044	1800	
PA	0.96	0.93	OA=0.943	

In order to make the distribution of impervious surfaces at the neighborhood scale comparable, impervious surface proportions were calculated for each neighborhood (Table 5). In this context, spatial comparison was made by determining the percentage of impervious surface areas in the total area.

CC: BY-NC-ND

Table 5. Neighborhood-level impervious surface proportions and changes between 2015 and 2025

		Impervious Surface (%)		Change (percentage points)
	Neighborhood Names	**2015**	**2025**	
1	Karapınar	28	35	+7
2	Cumhuriyet	27	62	+35
3	Karşıyaka	29	47	+18
4	Akyazı	60	66	+6
5	Bucak	36	45	+9
6	Durugöl	51	61	+10
7	Bahçelievler	71	74	+3
8	Aziziye	15	17	+2
9	Düz	86	87	+1
10	Şahincili	41	59	+18
11	Şirinevler	59	70	+11
12	Selimiye	49	50	+1
13	Yeni	82	81	-1
14	Zaferimilli	13	13	0
15	Subaşı	72	68	-4
16	Taşbaşı	42	42	0
17	Şarkiye	85	85	0
18	Saray	41	42	+1

To statistically evaluate the temporal change in impervious surface proportions, the paired differences between the 2015 and 2025 values of the 18 neighborhoods were first examined for normality. The Shapiro–Wilk test indicated that the paired differences deviated significantly from a normal distribution ($W = 0.816$, $p = 0.003$). Therefore, the impervious surface proportions of the two periods were compared using the Wilcoxon signed-rank test. The median impervious surface proportion increased from 45.5% in 2015 to 60.0% in 2025, while the mean values increased from 49.3% (SD = 23.2) to 55.8% (SD = 21.3). The Wilcoxon signed-rank test revealed a statistically significant difference between the 2015 and 2025 impervious surface proportions ($W = 111$, $p = 0.004$) (Table 6). Effect size ($r_{rb} = 0.842$) indicated a large effect in the direction of higher impervious surface proportions in 2025. Overall, these findings demonstrate that the increase observed across the neighborhoods represents a statistically significant temporal change rather than only a descriptive difference between the two periods.

Table 6. Statistical comparison of neighborhood-level impervious surface proportions between 2015 and 2025

Comparison	N	Median 2015 (%)	Median 2025 (%)	Wilcoxon W	p	Effect size
2025–2015	18	45.5	60.0	111	0.004	0.842

Note: The analysis included 18 neighborhoods. Three pairs with zero differences between 2015 and 2025 (Zaferimilli, Taşbaşı, and Şarkiye) were excluded from the Wilcoxon signed-rank calculation, resulting in 15 non-zero pairs used for the test.

At the individual neighborhood level, however, the magnitude and direction of change showed considerable spatial variation. While substantial increases in impervious surface proportions were observed in some neighborhoods, the change remained limited or was slightly negative in others. In Cumhuriyet Neighborhood, the impervious surface proportion increased from 27% in 2015 to 62% in 2025, corresponding to an increase of 35 percentage points. Similarly, increases of 18 percentage points (from 41% to 59%) and 11 percentage points (from 59% to 70%) were observed in Şahincili

CC: BY-NC-ND

and Şirinevler, respectively.

On the other hand, several neighborhoods exhibited only minor differences between the two observation dates. In particular, Düz (86% to 87%), Selimiye (49% to 50%), Yeni (82% to 81%), and Saray (41% to 42%) showed changes of only ±1 percentage point, while no change was observed in Zaferimilli, Taşbaşı, and Şarkiye. Given the classification accuracies obtained for the two dates, these very small differences should not necessarily be interpreted as meaningful physical changes. Subaşı showed a somewhat larger decrease of 4 percentage points; however, this decrease should also be interpreted cautiously in light of classification uncertainty. Therefore, these neighborhoods were considered relatively stable between 2015 and 2025.

The fact that high impervious surface proportions (85% and above) were preserved in Düz and Şarkiye neighborhoods in both periods shows that these areas are already densely built urban core areas.

In order to reveal the spatial change occurring on impervious surfaces in the 2015–2025 period, a general change map was created using the binary classification results of two periods (Figure 6).

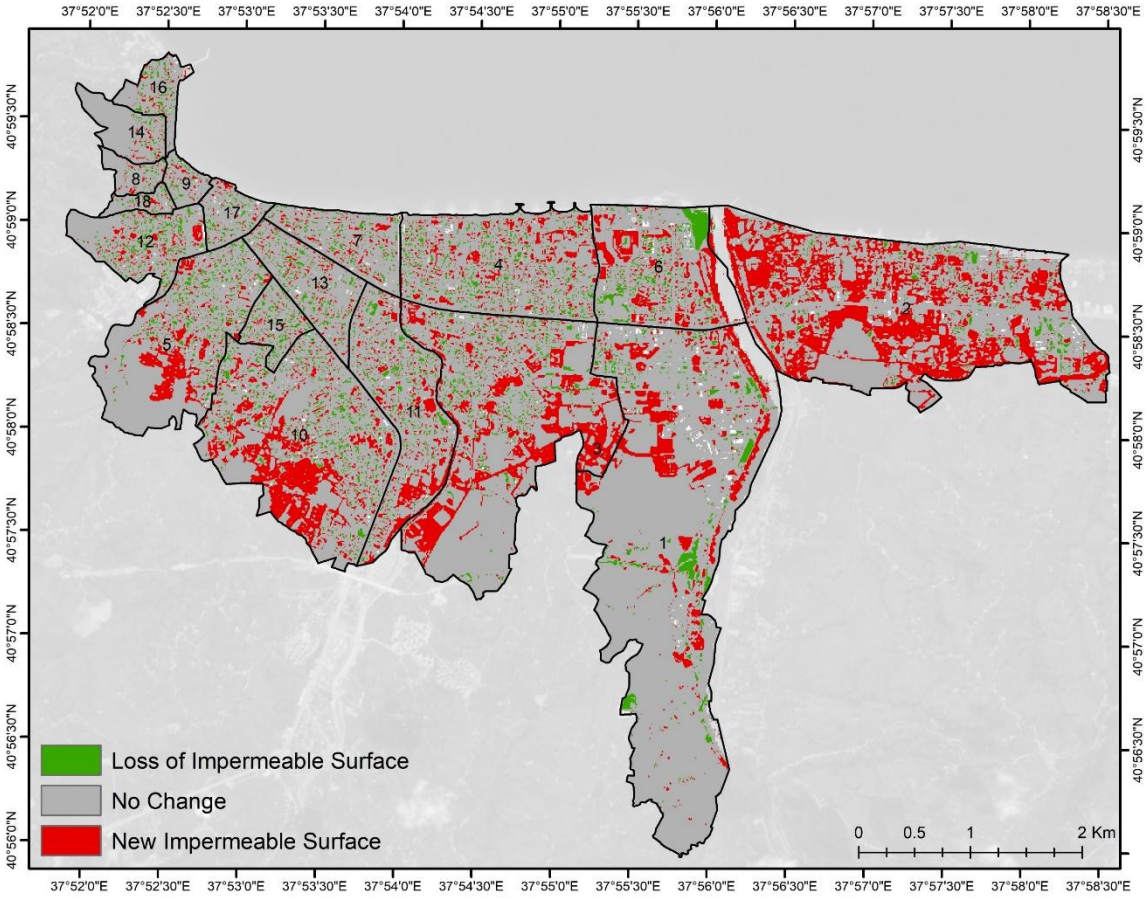

Figure 6. Spatial distribution of ENDISI-based impervious surface changes.

In order to evaluate the spatial patterns determined in the general change map in more detail, sample settlements representing neighborhoods where the increase in impervious surface was high, showed moderate change and remained relatively stable were selected. In this context, Cumhuriyet Neighborhood was considered as a sample area representing a high increase (+35 percentage points), Şahincili Neighborhood a moderate increase (+18 percentage points), and Şarkiye Neighborhood a relatively stable spatial structure (Figure 7).

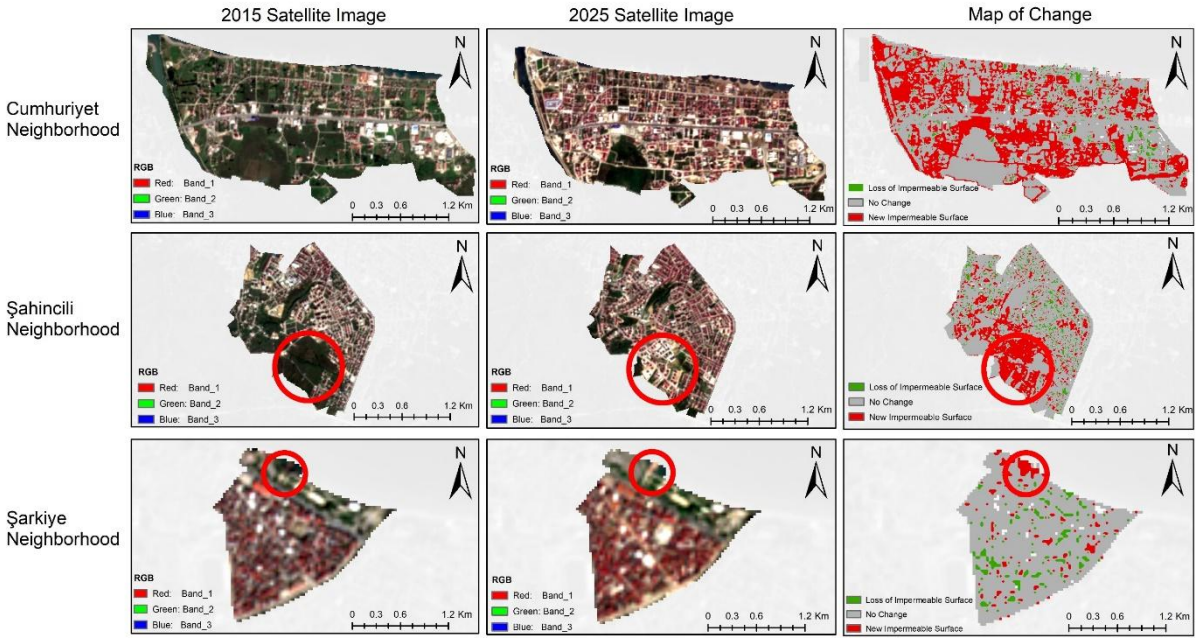

Figure 7. Spatial distribution of impervious surface changes of the determined neighborhoods

When the general change map and the comparative analyses carried out at the neighborhood scale are evaluated together, it is understood that the impervious surface changes in the study area show spatially different intensity and continuity characteristics. The findings reveal substantial neighborhood-level variation in impervious surface change, indicating that urban growth was spatially heterogeneous across the selected study area.

5. DISCUSSION AND CONCLUSION

The spatial distribution and temporal change of urban impervious surfaces are considered one of the important indicators for monitoring urbanization processes and evaluating urban environmental impacts [37]. Impervious surface determination studies carried out using remote sensing data enable effective and repeatable analyses in large areas and obtaining reliable results, especially thanks to the spectral information provided by medium-resolution multispectral satellite data [38,39,42]. In this context, Sentinel-2 images provide significant advantages in determining impervious surfaces due to their high spatial resolution and band diversity. Various studies have demonstrated that Sentinel-2 data can be used effectively in impervious surface mapping and can provide satisfactory accuracy levels, especially in heterogeneous urban textures [29-31].

Among the spectral indices used in determining impervious surfaces, ENDISI stands out especially in terms of its capacity to reduce the spectral mixing effect. In the comparative study conducted by Chen et al. (2020), it was determined that ENDISI produced higher discrimination and higher overall accuracy values than other built-up indices in different study areas [22]. According to the findings obtained in this study, the fact that SDI values are above 1 for both periods shows that ENDISI has sufficient spectral discrimination power to distinguish impervious and permeable surfaces. In addition, although the SDI value was numerically higher in 2025 than in 2015, both values remained within the same SDI performance category. This difference should not be attributed to a single factor, as spectral variability and image-acquisition conditions may also influence class separability. Therefore, the present analysis does not provide sufficient evidence to associate the higher SDI value specifically with increasing building density.

Studies conducted in the literature show that the performance of impervious surface indices may vary depending not only on the algorithm used but also on the spatial structure and land cover diversity of the study area [32,33]. Especially in coastal settlements, water surfaces, moist soil areas and mixed land cover components increase the spectral mixture and affect classification accuracy.

CC: BY-NC-ND

The main reason for choosing ENDISI is that commonly used built-up indices such as NDBI, IBI and the Built-up Area Extraction Index (BAEI) are more affected by water and moist soil surfaces in coastal areas and may overestimate or underestimate impervious surfaces; ENDISI reduces this spectral mixing effect by using the SWIR ratio and the MNDWI component together [22-24]. However, direct comparisons with different indices (e.g. NDBI, IBI, BAEI) in the same study area would more precisely reveal the impact of index choice on classification accuracy.

In this study, MNDWI-based masking was applied as a preprocessing step to minimize the potential spectral confusion between water and impervious surfaces in the coastal zone. However, because classification results with and without MNDWI masking were not comparatively evaluated, the specific effect of masking on classification performance cannot be quantified from the present analysis. The SDI values above 1 for both periods (2015: 1.36; 2025: 1.48), overall accuracies of 92.3–94.3%, and Kappa coefficients ranging from 0.84 to 0.88 indicate satisfactory performance of the overall classification procedure.

Neighborhood-scale analyses reveal that impervious surface changes were spatially heterogeneous, with the magnitude of change varying among the selected neighborhoods (Figure 8).

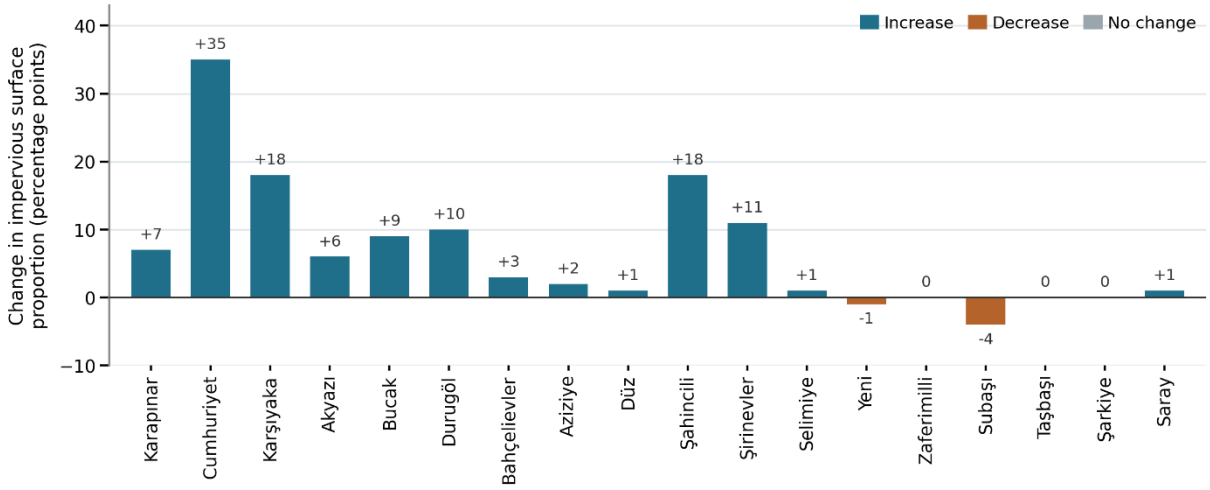

Figure 8. Neighborhood-level change in impervious surface proportions between 2015 and 2025 (percentage points)

While substantial increases in impervious surface proportions were observed in some neighborhoods, the magnitude of change remained limited in others. This shows that urban growth did not occur simultaneously and with equal intensity throughout the study area. Although similar spatial patterns have been reported by Liu et al. (2023) [34], the present study did not conduct an explicit corridor, directional, proximity, or hotspot analysis. Therefore, the spatial patterns observed in Altınordu are interpreted only as neighborhood-level differences and visual patterns in the change maps, as no formal spatial analysis was conducted to delineate specific directions or corridors of urban development.

The statistical analysis further supports the temporal pattern identified through the neighborhood-scale spatial assessment. The significant difference between the 2015 and 2025 impervious surface proportions (Wilcoxon signed-rank test, $p = 0.004$), together with the large rank-biserial effect size ($r_{rb} = 0.842$), indicates that the observed increase represents a systematic temporal shift across the analyzed neighborhoods rather than merely isolated changes in a limited number of locations. Nevertheless, this overall statistical tendency should be interpreted together with the pronounced spatial heterogeneity observed within the study area. While neighborhoods such as Cumhuriyet, Karşıyaka, and Şahincili experienced substantial increases, several already highly urbanized neighborhoods exhibited only limited change, and some neighborhoods remained stable or showed slight decreases. Thus, the statistically significant overall increase does not imply a spatially uniform transformation; rather, it reflects a spatially heterogeneous urbanization process in which the

CC: BY-NC-ND

magnitude of impervious surface expansion varies considerably among the selected neighborhoods.

The magnitude of impervious surface change observed in Altınordu can be further interpreted through comparison with findings reported for other coastal and tourism-oriented urban areas. In the coastal zone of Trabzon, Guneroglu (2015) reported that impervious surface area approximately doubled between 1984 and 2011, with the observed transformation being associated with the conversion of coastal agricultural land, linear-littoral urban development, and transportation infrastructure [43]. Similarly, Hua et al. (2023) reported that the proportion of impervious surface area in Xiamen, a rapidly urbanizing coastal city in China, increased from 16.33% to 26.17% between 2009 and 2021, corresponding to an increase of 9.84 percentage points [35]. Comparable development pressures have also been documented in tourism-oriented coastal areas of Türkiye. In the Belek Tourism Center, Akdeniz et al. (2023) reported that the proportion of built-up areas increased by 11.91 percentage points over the 1985–2021 period, demonstrating substantial tourism-related land-use transformation [44]. Furthermore, Tülek and Seçkin Gündoğan (2024) documented considerable urban expansion and land-cover transformation between 2007 and 2022 across the central districts of Antalya, one of Türkiye's major coastal tourism regions [45].

Against this comparative background, the changes detected in Altınordu should not be interpreted as uniformly high across the entire study area. Rather, they indicate a spatially heterogeneous urbanization pattern. In particular, the 35-percentage-point increase in Cumhuriyet and the 18-percentage-point increases in Karşıyaka and Şahincili between 2015 and 2025 indicate relatively rapid local transformation, whereas already highly urbanized neighborhoods such as Düz and Şarkiye exhibited very limited change. Although direct numerical comparisons should be approached cautiously because of differences among studies in terms of temporal coverage, spatial scale, satellite data, land-cover definitions, and classification methods, the magnitude of change observed in these neighborhoods indicates substantial local-scale transformation in impervious surface proportions. Therefore, the distinctive characteristic observed in Altınordu is the marked neighborhood-level variation in impervious surface change within a spatially heterogeneous coastal urban setting.

The spatial differences observed in impervious surface change may reflect broader urban development processes operating within the study area. Factors such as population growth, spatial planning decisions, transportation infrastructure development, and the formation of new construction areas may provide contextual explanations for the observed spatial patterns, as similar relationships have been discussed in previous studies [35]. However, these factors were not explicitly incorporated as explanatory variables in the present analytical design. Therefore, the observed neighborhood-level differences should not be interpreted as evidence of statistical or causal relationships between these drivers and impervious surface change. Further studies integrating demographic, transportation, and planning-related variables are needed to examine these potential relationships quantitatively.

The ENDISI-based classification showed satisfactory performance within the Altınordu study area, as supported by the accuracy assessment results obtained for both observation years. These findings demonstrate the applicability of ENDISI under the specific spatial and land-cover conditions represented by the selected urban neighborhoods of Altınordu. However, the present single-city case study does not provide sufficient evidence to generalize this performance to other medium-sized coastal cities or heterogeneous coastal settlements. Such broader applicability would require validation across multiple cities and contrasting urban and environmental contexts.

When the findings obtained are evaluated together, it is seen that addressing impervious surface changes not only in terms of total area increase but also in terms of spatial distribution patterns is important for understanding urban development processes. In this context, the present study provides a case-specific empirical assessment of neighborhood-level impervious surface change within the selected urban settlement belt of Altınordu and contributes to understanding spatial differences among the analyzed neighborhoods.

Because the analysis was restricted to 18 neighborhoods within the main urban settlement belt, the findings characterize impervious surface change within the selected urban area and should not be

CC: BY-NC-ND

interpreted as representative of the entire administrative district of Altınordu. Although Sentinel-2 images provide a suitable data source for monitoring impervious surfaces at the neighborhood scale, they have some limitations in representing small-scale building components and narrow urban details due to the 10 m spatial resolution. In the study, change was evaluated over two periods representing the beginning (2015) and ending (2025) of the ten-year period. This choice was made to highlight the clear spatial change that occurred throughout the period and to work with suitable, comparable summer period images in terms of cloud cover. Including intermediate years in the analysis will reveal the temporal continuity of impervious surface change in more detail and is recommended for future studies. In addition, the fact that the threshold value determination process was carried out on a sampling basis shows that there may be limited differences in the results if different threshold determination approaches are applied. Therefore, in future studies, evaluating higher spatial resolution satellite data and multi-temporal analyses together will contribute to revealing impervious surface change processes in more detail. In addition, evaluating impervious surface changes together with population development, transportation infrastructure and planning decisions will allow a more holistic understanding of urban development dynamics.

In addition, very small differences in neighborhood-level impervious surface proportions should be interpreted cautiously in relation to classification uncertainty. Although the classifications achieved overall accuracies of 92.3% for 2015 and 94.3% for 2025, these accuracy measures do not imply that differences of only one or a few percentage points necessarily represent detectable physical changes. Such minor differences may partly reflect classification variability, spectral variability, or spatial-resolution effects. Accordingly, neighborhoods exhibiting only minimal differences between the two dates were interpreted as relatively stable rather than as showing definitive increases or decreases in impervious surfaces.

Peer-review: External, Independent.

Acknowledgements:

-

Declarations:

1. Statement of Originality:

This work is original.

2. Author Contributions:

Concept: MY,EŞ; ***Conceptualization:*** MY,EŞ; ***Literature Search:*** MY,EŞ; ***Data Collection:*** MY,EŞ; ***Data Processing:*** MY,EŞ; ***Analysis:*** MY,EŞ; ***Writing – original draft:*** MY,EŞ; ***Writing – review & editing:*** MY,EŞ.

3. Ethics approval:

Not applicable.

4. Funding/Support:

This work has not received any funding or support.

5. Competing Interests:

The authors declare no competing interests.

6. GenAI Usage Statement:

Generative AI tools were used for language editing and for improving the clarity of the English text during manuscript revision. No generative AI tool was used to acquire or process the satellite imagery, to produce the classification or accuracy assessment results, to perform the statistical analyses, or to formulate the scientific interpretations.

7. Sustainable Development Goals:

CC: BY-NC-ND

REFERENCES

[1] Chithra, S. V., Harindranathan Nair, M. V., Amarnath, A., & Anjana, N. S. (2015). Impacts of impervious surfaces on the environment. International Journal of Engineering Science Invention, 4(5), 27–31. http://www.ijesi.org/papers/Vol(4)5/E045027031.pdf

[2] Sun, Z., Wang, C., Guo, H., & Shang, R. (2017). A Modified Normalized Difference Impervious Surface Index (MNDISI) for Automatic Urban Mapping from Landsat Imagery. Remote Sensing, 9(9), 942. https://doi.org/10.3390/rs9090942

[3] Weng, Q. (2012). Remote sensing of impervious surfaces in the urban areas: Requirements, methods, and trends. Remote Sensing of Environment, 117, 34-49. https://doi.org/10.1016/j.rse.2011.02.030

[4] Sun, Z., Li, X., Fu, W., Li, Y., & Tang, D. (2014). Long-term effects of land use/land cover change on surface runoff in urban areas of Beijing, China. Journal of Applied Remote Sensing, 8(1), 084596-084596. https://doi.org/10.1117/1.JRS.8.084596

[5] Mathew, A., Khandelwal, S., & Kaul, N. (2016). Spatial and temporal variations of urban heat island effect and the effect of percentage impervious surface area and elevation on land surface temperature: Study of Chandigarh city, India. Sustainable Cities and Society, 26, 264-277. https://doi.org/10.1016/j.scs.2016.06.018

[6] Melesse, A. M., Weng, Q., Thenkabail, P. S., & Senay, G. B. (2007). Remote Sensing Sensors and Applications in Environmental Resources Mapping and Modelling. Sensors, 7(12), 3209-3241. https://doi.org/10.3390/s7123209

[7] Seto, K. C., Fragkias, M., Güneralp, B., & Reilly, M. K. (2011). A meta-analysis of global urban land expansion. PLoS ONE, 6(8), e23777. https://doi.org/10.1371/journal.pone.0023777

[8] Xu, J., Zhao, Y., Zhong, K., Zhang, F., Liu, X., & Sun, C. (2018). Measuring spatio-temporal dynamics of impervious surface in Guangzhou, China, from 1988 to 2015, using time-series Landsat imagery. Science of the Total Environment, 627, 264-281. https://doi.org/10.1016/j.scitotenv.2018.01.155

[9] Santangelo, J. S., Ness, R. W., Cohan, B., Fitzpatrick, C. R., Innes, S. G., Koch, S., ... & Lampei, C. (2022). Global urban environmental change drives adaptation in white clover. Science, 375(6586), 1275-1281. DOI: 10.1126/science.abk0989

[10] Franke, J., Roberts, D. A., Halligan, K., & Menz, G. (2009). Hierarchical multiple endmember spectral mixture analysis (MESMA) of hyperspectral imagery for urban environments. Remote Sensing of Environment, 113(8), 1712-1723. https://doi.org/10.1016/j.rse.2009.03.018

[11] Zhao, Y., Xu, J., Zhong, K., Wang, Y., Hu, H., & Wu, P. (2020). Impervious surface extraction by linear spectral mixture analysis with post-processing model. IEEE Access, 8, 128476-128489. DOI: 10.1109/ACCESS.2020.3008695

[12] Shao, Z., Cheng, T., Fu, H., Li, D., & Huang, X. (2023). Emerging Issues in Mapping Urban Impervious Surfaces Using High-Resolution Remote Sensing Images. Remote Sensing, 15(10), 2562.

https://doi.org/10.3390/rs15102562

[13] Sun, Z., Guo, H., Li, X., Lu, L., & Du, X. (2011). Estimating urban impervious surfaces from Landsat-5 TM imagery using multilayer perceptron neural network and support vector machine. Journal of Applied Remote Sensing, 5(1), 053501-053501. https://doi.org/10.1117/1.3539767

[14] Su, S., Tian, J., Dong, X., Tian, Q., Wang, N., & Xi, Y. (2022). An Impervious Surface Spectral Index on Multispectral Imagery Using Visible and Near-Infrared Bands. Remote Sensing, 14(14), 3391. https://doi.org/10.3390/rs14143391

[15] Kebede, T. A., Hailu, B. T., & Suryabhagavan, K. V. (2022). Evaluation of spectral built-up indices for impervious surface extraction using Sentinel-2A MSI imageries: A case of Addis Ababa city, Ethiopia. Environmental Challenges, 8, 100568. https://doi.org/10.1016/j.envc.2022.100568

[16] Ahmad, M. N., Shao, Z., & Javed, A. (2023). Mapping impervious surface area increase and urban pluvial flooding using Sentinel Application Platform (SNAP) and remote sensing data. Environmental Science and Pollution Research, 30(60), 125741-125758. https://doi.org/10.1007/s11356-023-30990-y

[17] Dvornikov, Y., Grigorieva, V., Varentsov, M., & Vasenev, V. (2023). Optimal spectral index and threshold applied to Sentinel-2 data for extracting impervious surface: Verification across latitudes, growing seasons, approaches, and comparison to global datasets. International Journal of Applied Earth Observation and Geoinformation, 123, 103470. https://doi.org/10.1016/j.jag.2023.103470

[18] Wu, W., Guo, S., Shao, Z., & Li, D. (2023). Urban Impervious Surface Extraction Based on Deep Convolutional Networks Using Intensity, Polarimetric Scattering and Interferometric Coherence Information from Sentinel-1 SAR Images. Remote Sensing, 15(5), 1431. https://doi.org/10.3390/rs15051431

[19] Lefebvre, A., Sannier, C., & Corpetti, T. (2016). Monitoring Urban Areas with Sentinel-2A Data: Application to the Update of the Copernicus High Resolution Layer Imperviousness Degree. Remote Sensing, 8(7), 606. https://doi.org/10.3390/rs8070606

[20] Ding, Y., Ding, Q., Yang, J., Shao, Z., & Huang, X. (2022). PRISI: A novel piecewise radar impervious surface index for urban monitoring using Sentinel-1 data. International Journal of Applied Earth Observation and Geoinformation, 114, 103033. https://doi.org/10.1016/j.jag.2022.103033

[21] Yang, X., Zhao, S., Qin, X., Zhao, N., & Liang, L. (2017). Mapping of Urban Surface Water Bodies from Sentinel-2 MSI Imagery at 10 m Resolution via NDWI-Based Image Sharpening. Remote Sensing, 9(6), 596. https://doi.org/10.3390/rs9060596

[22] Chen, J., Chen, S., Yang, C., He, L., Hou, M., & Shi, T. (2020). A comparative study of impervious surface extraction using Sentinel-2 imagery. European Journal of Remote Sensing, 53(1), 274–292. https://doi.org/10.1080/22797254.2020.1820383

[23] Chen, Y., Ge, Y., An, R., & Chen, Y. (2018). Super-Resolution Mapping of Impervious Surfaces from Remotely Sensed Imagery with Points-of-Interest. Remote Sensing, 10(2), 242. https://doi.org/10.3390/rs10020242

[24] Yücer, E. (2025). Determination of impervious surface areas using remote sensing indices: a case of Ankara. Episodes Journal of International Geoscience, 48(3), 279-294. https://doi.org/10.18814/epiiugs/2024/024027

[25] Pereira, J. M. (1999). A comparative evaluation of NOAA/AVHRR vegetation indexes for burned surface detection and mapping. IEEE Transactions on Geoscience and Remote Sensing, 37(1), 217-226. DOI: 10.1109/36.739156

CC: BY-NC-ND

[26] Deng, Y., Wu, C., Li, M., & Chen, R. (2015). RNDSI: A ratio normalized difference soil index for remote sensing of urban/suburban environments. International Journal of Applied Earth Observation and Geoinformation, 39, 40-48. https://doi.org/10.1016/j.jag.2015.02.010

[27] Kaufman, Y. J., & Remer, L. A. (1994). Detection of forests using mid-IR reflectance: An application for aerosol studies. IEEE Transactions on Geoscience and Remote Sensing, 32(3), 672-683.

[28] Batra, U., Roy, N. R., & Panda, B. (Eds.). (2020). Data Science and Analytics: 5th International Conference on Recent Developments in Science, Engineering and Technology, REDSET 2019, Gurugram, India, November 15–16, 2019, Revised Selected Papers, Part II.

[29] Kuc, G., & Chormański, J. (2019). Sentinel-2 imagery for mapping and monitoring imperviousness in urban areas. The International Archives of the Photogrammetry, Remote Sensing and Spatial Information Sciences, 42, 43-47. https://doi.org/10.5194/isprs-archives-XLII-1-W2-43-2019

[30] Giacco, G., Marrone, S., Langella, G., & Sansone, C. (2022). ReFuse: Generating Imperviousness Maps from Multi-Spectral Sentinel-2 Satellite Imagery. Future Internet, 14(10), 278. https://doi.org/10.3390/fi14100278

[31] Feng, X., Shao, Z., Huang, X., He, L., Lv, X., & Zhuang, Q. (2022). Integrating Zhuhai-1 hyperspectral imagery with Sentinel-2 multispectral imagery to improve high-resolution impervious surface area mapping. IEEE Journal of Selected Topics in Applied Earth Observations and Remote Sensing, 15, 2410-2424.

[32] Fang, H., Wei, Y., & Dai, Q. (2019). A Novel Remote Sensing Index for Extracting Impervious Surface Distribution from Landsat 8 OLI Imagery. Applied Sciences, 9(13), 2631. https://doi.org/10.3390/app9132631

[33] Xu, F., Heremans, S., & Somers, B. (2022). Urban land cover mapping with Sentinel-2: A spectro-spatio-temporal analysis. Urban Informatics, 1(1), 8. https://doi.org/10.1007/s44212-022-00008-y

[34] Liu, J., Zhang, Y., Liu, C., & Liu, X. (2023). Monitoring Impervious Surface Area Dynamics in Urban Areas Using Sentinel-2 Data and Improved Deeplabv3+ Model: A Case Study of Jinan City, China. Remote Sensing, 15(8), 1976. https://doi.org/10.3390/rs15081976

[35] Hua, L., Wang, H., Zhang, H., Sun, F., Li, L., & Tang, L. (2023). A New Technique for Impervious Surface Mapping and Its Spatio-Temporal Changes from Landsat and Sentinel-2 Images. Sustainability, 15(10), 7947. https://doi.org/10.3390/su15107947

[36] Matpay, B. (2026). Uzaktan Algılama ve CBS Teknikleri ile Erçek Gölü (Van) Kıyı Çizgisinin Mekânsal-Zamansal Değişim Analizi (1984–2025). Geomatik, 11(2), 266-276. https://doi.org/10.29128/geomatik.1927188

[37] Demirdağ, G. E., & Cubukcu, K. M. (2025). Mapping Urban Growth Through Landscape Expansion Index and Land Use Analysis: Evidence from Western Turkey. International Journal of Engineering and Geosciences, 11(2), 252-262. https://doi.org/10.26833/ijeg.1659422

[38] Ambreen, H., & Rahman, A. U. (2025). Evaluating spatio-temporal dynamics in LULC and its implications on land surface temperature of Swat valley, Eastern Hindukush. International Journal of Engineering and Geosciences, 10(3), 495-503. https://doi.org/10.26833/ijeg.1666208

[39] Tomco, V., Grabocka, E., & Harizaj, M. (2025). Leveraging Deep Learning in Remote Sensing: A Novel Approach for Agricultural Greenhouse Detection and Innovation Management. International Journal of Engineering and Geosciences, 10(2), 221-230. https://doi.org/10.26833/ijeg.1587264

CC: BY-NC-ND

[40] Baytar, İ. (2025). Arazi Kullanımının Coğrafi Bilgi Sistemleri (CBS) ile Haritalanması ve Analizi: Van Şehri Örneği. Geomatik, 11(1), 1-16. https://doi.org/10.29128/geomatik.1673220

[41] Yaman, Ş., & Tunç Görmüş, E. (2025). Sentinel-2 ve Landsat-8 ile Bulut Tabanlı Orman Yangın Analizi. Geomatik, 10(3), 316-330. https://doi.org/10.29128/geomatik.1603707

[42] Karakoca, E., & Ünver, A. (2025). Analitik hiyerarşi süreci ve coğrafi bilgi sistemleri kullanarak Eşen Çayı Havzası'nda taşkın riski değerlendirmesi ve haritalandırılması. Geomatik, 10(1), 127-143. https://doi.org/10.29128/geomatik.1542251

[43] Guneroglu, A. (2015). Coastal changes and land use alteration on Northeastern part of Turkey. Ocean & Coastal Management, 118, 225–233. https://doi.org/10.1016/j.ocecoaman.2015.06.019

[44] Akdeniz, H. B., Serdaroglu Sag, N., & Inam, S. (2023). Analysis of land use/land cover changes and prediction of future changes with land change modeler: Case of Belek, Turkey. Environmental Monitoring and Assessment, 195, 135. https://doi.org/10.1007/s10661-022-10746-w

[45] Tülek, B., & Seçkin Gündoğan, G. (2024). Impact of land surface temperature variability and population growth on ecosystem services in the central districts of Antalya. Ain Shams Engineering Journal, 15, 103140. https://doi.org/10.1016/j.asej.2024.103140

[46] Li, Y., Meng, D., Yang, Q., Zhang, M., & Zhao, Y. (2026). Inversion of Soil Arsenic Concentration in Sanlisha'an Mining Area Based on ZY-02E Hyperspectral Satellite Images. Remote Sensing, 18(5), 822. https://doi.org/10.3390/rs18050822

CC: BY-NC-ND